THE ASTROPHYSICAL JOURNAL, 542:359–366, 2000 October 10

HIGH-RESOLUTION IMAGING OF PHOTODISSOCIATION REGIONS IN NGC 6334

M. G. BURTON, M. C. B. ASHLEY, R. D. MARKS,[1] A. E. SCHINCKEL,[2] AND J. W. V. STOREY
School of Physics, University of New South Wales, Sydney, NSW 2052, Australia
A. FOWLER, M. MERRILL, AND N. SHARP
National Optical Astronomy Observatory, P.O. Box 26732, Tucson, AZ 85726-6732
I. GATLEY
Chester F. Carlson Center for Imaging Science, Rochester Institute of Technology, Rochester, NY 14623-5604
D. A. HARPER, R. F. LOEWENSTEIN, AND F. MROZEK
University of Chicago, Yerkes Observatory, Williams Bay, WI 53191
AND
J. M. JACKSON AND K. E. KRAEMER[3]
Boston University, Department of Astronomy, Boston, MA 02215
Received 2000 January 10; accepted 2000 May 18

ABSTRACT

We have used the SPIREX telescope to conduct a wide-field thermal infrared imaging study of the star formation complex NGC 6334 in the southern Galactic plane. We imaged a 30′ region along the main star-forming ridge of NGC 6334 with 0.″6 pixel scale through broadband filters for L (3.5 μm) and M (4.8 μm) and through narrowband filters for the H_2 $v = 1$–0 Q-branch (2.42 μm), polycyclic aromatic hydrocarbon (PAH) (3.3 μm), and Brα (4.05 μm) lines. The images reveal the spectacular, complex structure of the photodissociation regions (PDRs) that pervade the region, with enhanced line emission around each of the seven sites of massive star formation along the ridge. Bubbles and loops of PAH emission, typically 1–1.5 pc across, have been carved out of the parent molecular cloud by the intense UV radiation from the massive stars and surround H II regions (seen in Brα) typically 0.2–0.3 pc across. The PAH emission regions coincide with both [C II] 158 μm line emission, indicating that the PAHs are excited in PDR gas, and extensive H_2 emission, which therefore must be fluorescent. However, the textures of the emission regions in PAH and H_2 are different. This is attributable to variations in the physical environment in which the gas is excited. Several compact reddened objects are observed; these are likely to be massive protostars.

Subject headings: infrared: general — infrared: ISM: lines and bands — ISM: molecules — ISM: structure — stars: formation — telescopes

1. INTRODUCTION

Most of the molecular gas in the Galaxy exists near photodissociation regions (PDRs), where far-UV radiation (6 eV $< h\nu <$ 13.6 eV) drives both the heating and the chemistry. Since most of the cooling radiation is emitted at far-IR wavelengths, as continuum from thermally heated dust and as line emission predominantly from [O I] 63 μm and [C II] 158 μm, investigation of PDR structure has largely involved low spatial resolution observations. It is clear that the overall morphology of PDRs generally conforms to theoretical expectations (e.g., Tielens & Hollenbach 1985), viz., a shell-like structure with successive layers containing ionized gas, then neutral photodissociated gas, and finally molecular gas, as the distance from an exciting source increases. However, the actual environment is rather heterogeneous. The observed line emission from even individual PDRs must arise from a range of densities and varying strength radiation fields (e.g., Stutzki et al. 1988) if it is to be reconciled with theoretical models. Since much of the energy transfer that takes place between stars and gas occurs in PDRs, understanding their internal structure is important in determining their role in regulating the star formation process.

NGC 6334 is a laboratory where PDRs can be studied in a range of environments. Located 1700 pc away in the southern Galactic plane, it is associated with an optical nebula $\sim 15 \times 30$ pc across (Rodgers, Campbell, & Whiteoak 1960). Several distinct sites[4] of massive star formation lie within the complex, as evidenced by separate far-IR and radio continuum sources characteristic of embedded massive stars (McBreen et al. 1979; Rodríguez, Cantó, & Moran 1982; Loughran et al. 1986) and by associated phenomena such as PDRs, H II regions, outflows, and masers (see Jackson & Kraemer 1999 and references therein). The OB stars range in spectral type from B0 to O6 and are about 2′ (1 pc) apart, aligned along a molecular ridge which

[1] Rodney Marks tragically died of natural causes while working at the South Pole on 2000 May 12. He was spending his second winter there, operating the AST/RO submillimeter telescope. Rodney spent the winter of 1998 at the Pole operating the SPIREX telescope. His perseverance and dedication, overcoming considerable difficulties through the Antarctic winter, were crucial to obtaining the results presented in this paper. Rodney's pioneering efforts have shown that infrared astronomy in Antarctica can be a reality, not just a dream. We dedicate this paper to Rodney's memory.

[2] Current address: Smithsonian Astrophysical Observatory, Center for Astrophysics, 60 Garden Street, Cambridge, MA 02138.

[3] Current address: AFRL/VSBC, 29 Randolph Road, Hanscom AFB, MA 01731.

[4] We use the source designations of McBreen et al. (1979) for the far-IR continuum sources NGC 6334:MFSW I, II, III, IV, and V, and the notation of Gezari (1982) for the millimeter continuum source NGC 6334:MFSW I(N). For succinctness, these are abbreviated as sources I, II, etc.

extends $\sim 20' \times 3'$ and bisects the optical nebula. These stars have a spread of both evolutionary stages and radiation fields. This provides an opportunity to observe the different characteristics of the PDRs within the complex while factors such as distance and age of the parent molecular cloud are constant. Of particular interest is the source NGC 6334 V at the southwest end of the molecular ridge, for which the estimates for stellar type based on IR luminosity (O8.5) and radio continuum (B2) are widely disparate, suggesting that it may be a massive protostar.

Figure 1, a schematic of NGC 6334, shows the locations of the six far-IR sources I(N) and I–V, arranged northeast-southwest along the molecular ridge, and the radio continuum sources [RCM82] NGC 6334:A–F (Rodríguez et al. 1982), arranged southwest-northeast along it, overlaid on the CO (2–1) image from Kraemer & Jackson (1999).

High spatial resolution imaging of the structure of PDRs is best done with wide-field imaging in the thermal portion of the near-IR, from 2.4 to 5 μm. The PDR interface is delineated by the 3.3 μm polycyclic aromatic hydrocarbon (PAH) emission feature, fluorescently excited by far-UV radiation (Tielens et al. 1993). Brα emission at 4.05 μm identifies ionized gas, with reddening normally minimal. H_2 emission from the $v = 1$–0 Q-branch lines at 2.4 μm traces the molecular gas at an optical depth $A_v \sim 1$ in from the interface (Burton, Hollenbach, & Tielens 1990). Observations of PDRs in this wavelength regime have been hindered by the poor sensitivity of ground-based telescopes, arising from the strong thermal emission of the atmosphere and its moderate and variable transmission. Dry and exceedingly cold sites, such as found on the Antarctic plateau, where IR sky backgrounds can fall by 20 times below those of good temperate latitude sites (Ashley et al. 1996; Nguyen et al. 1996; Phillips et al. 1999; Chamberlain et al. 2000), offer a significant advantage for such work. We report in this paper the first such results from the SPIREX/Abu IR telescope at the South Pole, which has been designed for wide-field imaging in the thermal part of the near-IR.

2. OBSERVATIONS

SPIREX is a 60 cm telescope built in 1994 for operation at the South Pole (Hereld et al. 1990). It was equipped in 1998 with the NOAO Abu IR camera (Fowler et al. 1998), which incorporates an engineering grade 1024×1024 "Aladdin" InSb 1–5 μm array, able to image a $10\farcm2 \times 10\farcm2$ circular field of view at $0\farcs6$ pixel scale through discrete filters. These cover three lines, H_2 $v = 1$–0 Q-branch (2.42 μm), PAH (3.3 μm), and Brα (4.05 μm), with narrowband (1%–2% width) filters and L (3.5 μm), L' (3.8 μm), and M (4.7 μm) with broadband continuum filters. The low sky background at the South Pole makes it possible to use broadband filters for continuum measurements, unlike at temperate sites. The diffraction limit of the telescope at 3.5 μm is $1\farcs5$, comparable to the typical ice-level seeing of the site. When the unguided observations are combined with tracking errors, tower shake, and the co-addition of frames over a 2–3 hr interval, the typical resolution obtained is $3''$–$4''$. However, short test exposures achieved the diffraction limit of the telescope.

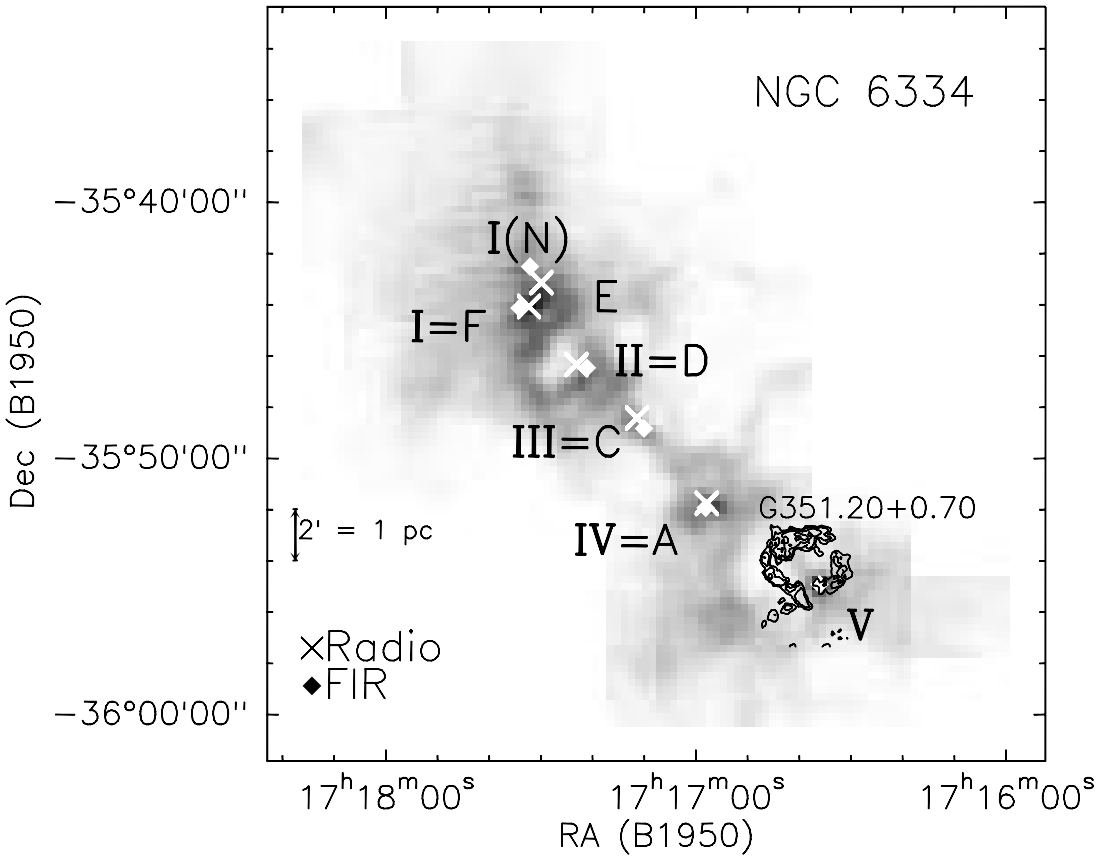

FIG. 1.—CO (2–1) emission from NGC 6334, adapted from Kraemer & Jackson (1999). Darker is more intense. Compact continuum sources indicated: radio sources (*crosses*, alphabetical names A–F; Rodríguez et al. 1982), far-IR and submillimeter sources (*filled diamonds*, Roman numerals; McBreen et al. 1979). Also shown is the 3 cm continuum emission from the diffuse radio source G351.20+0.70 (*contours*; Jackson & Kraemer 1999; Moran et al. 1990).

During the austral winter of 1998, NGC 6334 was imaged through these filters at three overlapping locations (northeast: $17^h17^m33^s$, $-35°44'00''$; central: $17^h17^m7^s.6$, $-35°49'35''$; southwest: $17^h16^m40^s.6$, $-35°55'00''$ [1950]). A typical observing sequence consisted of a five-position cross, separated by 30″ per position, each with 2–3 minutes of integration, followed by a similar sequence on an off-source position up to a degree away. This sequence was repeated for a total on-source integration time of 2–3 hr. Data reduction consisted of bias subtraction, flat-fielding using an archival flat, and sky subtraction from an appropriately determined median sky frame. Depending on whether a program is aimed at point-source photometry or extended, diffuse imaging, sky frames might be determined from the nearest frames in time or from just the off-source frames. Frames were then mosaicked using a mask image to eliminate bad pixels. Figure 2 shows a three-color image of the NGC 6334 molecular ridge showing PAH emission (*blue*), *L*-band continuum (*green*), and Brα emission (*red*). This is the largest image ever obtained in the thermal-IR at this spatial resolution. Point-source sensitivities achieved over long integrations were (3 σ, 1 hr, 5″ × 5″) 6×10^{-18} W m^{-2} (H_2 Q), 1 mJy (PAH), 14.6 mag (L band), 5×10^{-17} W m^{-2} (Brα), and 10.2 mag (M band). While these figures are typically up to 1 mag worse than the theoretical performance for the site (during 1998 the instrument suffered from excess thermal radiation from a support structure), at L band the sensitivity is over 5 mag better than has been achieved with the MOSAIC camera on the KPNO 4 m telescope, while providing a field of view some 20 times

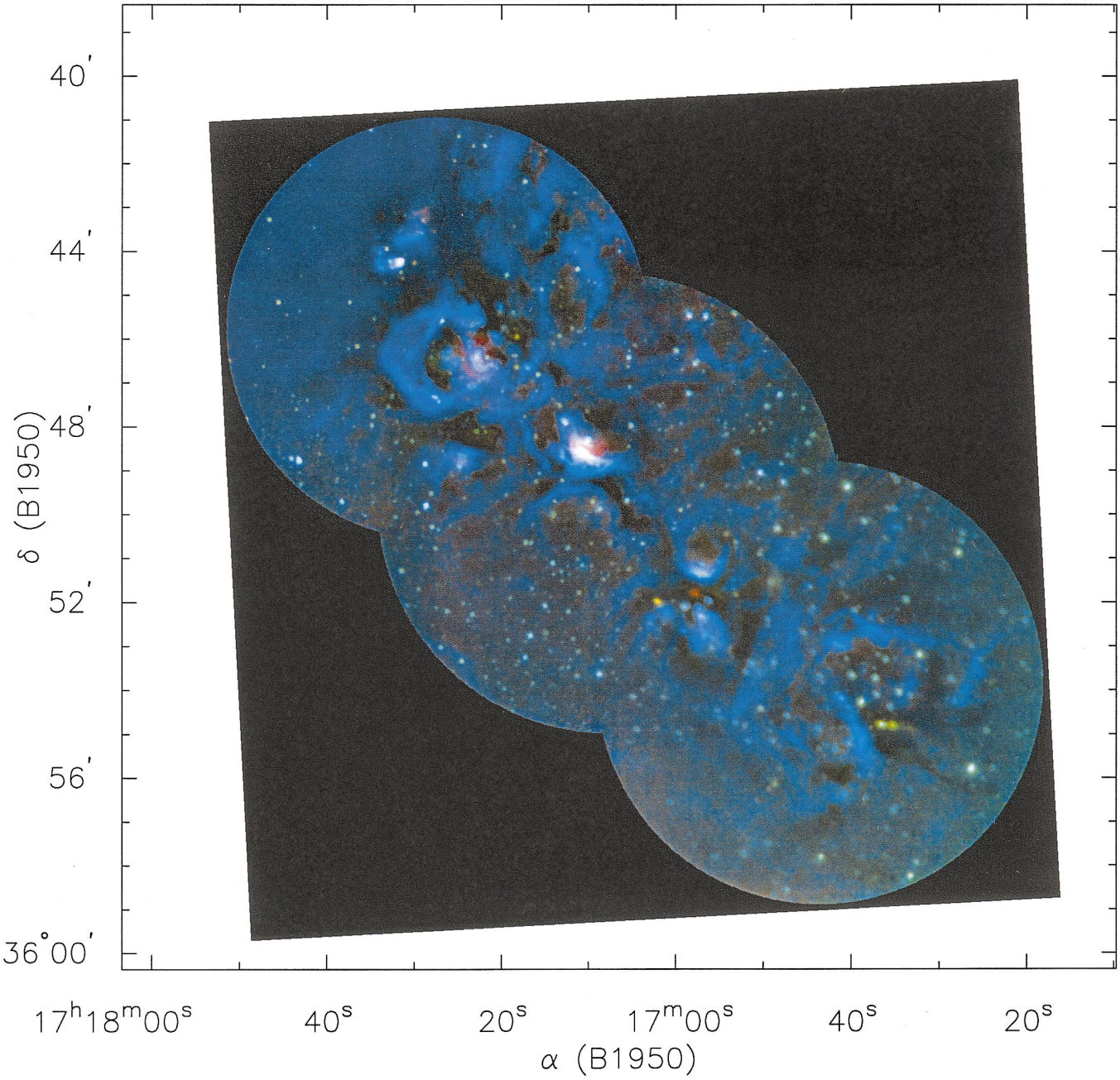

FIG. 2.—Three-color infrared image of a 30′ section of the molecular ridge of NGC 6334 (*blue*: 3.3 μm PAH; *green*: 3.5 μm L band; *red*: 4.05 μm Brα) obtained with the SPIREX/Abu telescope at the South Pole.

larger. Figure 3 is a three-color optical image from the Schmidt telescope at Siding Spring (Malin 1993), with the region of the SPIREX/Abu image, along the dark lane which bisects the optical nebula, indicated.

3. RESULTS

3.1. *Morphology*

Figure 2 shows the spectacular, complex structure of the PDRs along the molecular ridge of NGC 6334. While PAH emission covers the field, strong enhancements are seen connected with the regions around each of the far-IR sources I–V. These are bubbles and loops which have been carved out of the parent molecular cloud by the intense radiation field from the massive stars sited along the molecular ridge. Each shell is typically 2′–3′ across, or 1–1.5 pc in size. The shells lie outside ionized bubbles, evident through their Brα emission and also through thermal radio continuum emission at 8.5 GHz (Jackson & Kraemer 1999). The compact H II regions they surround are typically only 0.2–0.3 pc across.

The PAH emission traces the same regions seen in [C II] 158 μm, as seen in Figure 4, where it is overlaid with the [C II] image from Kraemer (1998), albeit at vastly different spatial resolutions. Since [C II] 158 μm is an unambiguous tracer of PDRs, it indicates that the PAH image is likely tracing the region of photodissociated gas on arcsecond (0.01 pc) spatial scales.

FIG. 3.—Color image of NGC 6334 obtained with the Schmidt telescope at Siding Spring Observatory (Malin 1993) through blue, green, and red filters, with the region observed with SPIREX/Abu outlined.

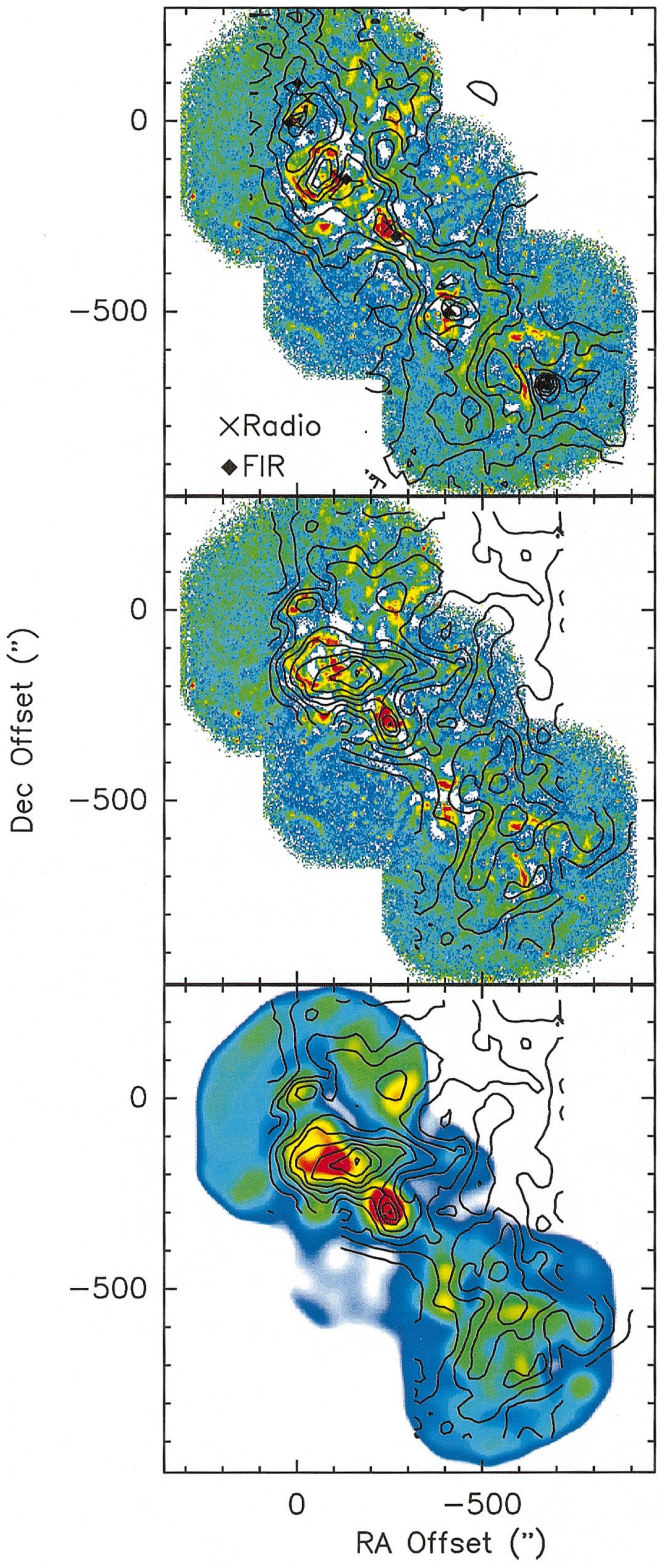

FIG. 4.—The PAH 3.3 μm emission compared with the CO (2–1) (Kraemer & Jackson 1999) and [C II] 158 μm (Kraemer et al. 1999). Offsets, in arcseconds, are relative to radio source F (far-IR source I), at $17^h17^m32^s.3$, $-35°44'04''$ (1950). Top: PAH 3.3 μm (*log color scale*, resampled to 2".2 spacing) vs. CO (2–1) (*contours*, 100 K km s^{-1} intervals); center: PAH 3.3 μm (*log color scale*, resampled to 2".2 spacing) vs. [C II] 158 μm (*contours*, 10% of peak emission intervals); bottom: PAH 3.3 μm (*log color scale*, convolved with a 50" Gaussian beam, the resolution of the [C II] observations) vs. [C II] 158 μm (*contours*, 10% of peak emission intervals).

Equally noticeable in Figure 2 are the dark lanes parallel to the ridges and loops of PAH emission. These are generally on the other side of the PAH features to the ionized gas and thus are regions of increased extinction comprising ambient molecular gas that has not yet been subject to the dissociating UV radiation field. The dark lanes correspond to the locations of the molecular gas seen in, for instance, CO (2–1) (Kraemer & Jackson 1999) with a 26" beam (see also Fig. 4). Presumably, higher spatial resolution millimeter interferometry of the molecular lines would reveal a structure somewhat like that seen by the dark lanes in Figure 2.

There is one exception to the correspondence between the dark lanes and CO (2–1) line emission: the 30" wide dark arc that lies $\sim$1' to the east of source II. It is outside the 30" (0.3 pc) diameter bubble of Brα emission that surrounds 6334 D but *inside* the shell of PAH emission that extends a further 1' to the east. This region is also a hole in the CO line map (at approximately $-80''$, $-150''$; see Fig. 4, *top*). It therefore must mark a region devoid of gas, with a density-bounded bubble within it and a PDR outside it, being excited by the far-UV photons which have escaped the H II region. Since the O6 star (Straw & Hyland 1989a) that powers the H II region cannot have created this hole (otherwise it would be filled with ionized gas), the cavity must be preexisting. It is unlikely to have been created by another massive star formed earlier, as there is no evidence for such a source. Thus, this suggests that a cavity about 0.5 pc across must have remained within the natal giant molecular cloud which formed NGC 6334, providing evidence for an inhomogeneous cloud formation process.

Table 1 lists representative values for the 3.3 μm PAH flux from each of the far-IR sources I(N) and I–V. Peak fluxes are typically (10–30) $\times 10^{-17}$ W m^{-2} arcsec^{-2} over 2"–3" regions, with diffuse fluxes of (4–8) $\times 10^{-17}$ W m^{-2} arcsec^{-2} over 20"–60" regions around each source. Extended PAH emission, with fluxes of (2–3) $\times 10^{-17}$ W m^{-2} arcsec^{-2}, envelopes the entire molecular ridge. These are an order of magnitude higher than the H_2 Q-branch fluxes, which are of (2–4) $\times 10^{-18}$ W m^{-2} arcsec^{-2} across the region,[5] and are coextensive with the PAH emission. The line fluxes from the Brα-emitting bubbles, which are

[5] The Q-branch fluxes also have similar surface brightnesses to those reported by Straw & Hyland (1989b), measured through a 20" beam, indicating the diffuse nature of the H_2 line emission.

TABLE 1

REPRESENTATIVE LINE FLUXES IN NGC 6334

	3.3 μm PAH EMISSION		4.05 μm Brα EMISSION
FAR-IR SOURCE	Peak	Diffuse	Peak
I(N)	12	5	4
I	14	5	6
II	16	8	15
III	38	8	30
IV	29	7	10
V	14	4	3

NOTE.—All values shown are in units of 10^{-17} W m^{-2} arcsec^{-2}. Peak fluxes generally extend over 2"–3", whereas diffuse fluxes are over 20"–60" around each far-IR source. There is also extended PAH emission enveloping these, with a flux level of (2–3) $\times 10^{-17}$ W m^{-2} arcsec^{-2}. H_2 $v = 1$–0 Q-branch fluxes are in the range (2–4) $\times 10^{-18}$ W m^{-2} arcsec^{-2}.

surrounded by the shells of PAH emission, are in fact comparable to those of the PAHs, of order 10^{-16} W m^{-2} arcsec^{-2}.

Figure 5 presents images of the H_2, PAH, *L*-band, and Brα emission associated with the southwest position observed, which includes the far-IR sources IV and V. We discuss these further below.

3.2. *NGC 6334 IV*

Of particular note is the red source (Fig. 2) visible in the center of the dust lane associated with the far-IR source NGC 6334 IV (radio source NGC 6334:RCM A: Rodríguez et al. 1982) and coincident with mid-IR source [KDJ99] NGC 6334 IV 2 (hereafter KDJ-2: Kraemer et al. 1999; =[HHS87] IRS 19: Harvey, Hyland, & Straw 1987) (at $17^h16^m58^s$, $-35°51'43''$; see the Brα image in Fig. 5). Its central location, both in the dark lane and with respect to the shells of PAH emission north and south of the dark lane, suggests that it is the exciting source for the region. Kraemer et al. (1997) have shown that a 2000 $M_\odot$ rotating molecular disk also exists in source IV, coincident with the dark lane. However, Kraemer et al. (1999) suggest that the mid-IR source [KDJ99] NGC 6334 IV 3E (=[HHS87] IRS 20; hereafter KDJ-3E), 20″ west-southwest of KDJ-2, is also a massive protostar which contributes to the heating of the PDRs. This conjecture is based on KDJ-3E's 20 μm flux, which is brighter than that of KDJ-2, its lower color temperature, and its higher 12 μm optical depth. KDJ-2 is detected in the *L*-band filter and is particularly prominent in the Brα filter, whereas KDJ-3E is seen in the H_2 and PAH filters as well. However, it is not especially prominent in Brα. This would suggest that KDJ-2 is surrounded by an ultracompact H II region and is indeed the powering source for the PDR shells, as suggested by the morphology of the PAH and the dark lane. KDJ-3E, on the other hand, is an embedded IR source in a protostellar stage but has not yet started ionizing the surrounding cloud.

3.3. *NGC 6334 V*

The far-IR source NGC 6334 V is at the southwest end of the star-forming ridge, a region that is lacking in any bright radio continuum sources. An incomplete radio shell at 3.5 cm (G351.20+0.70: Moran et al. 1990; Fig. 1), 150″ across (1.3 pc), (Jackson & Kraemer 1999), apparently is centered

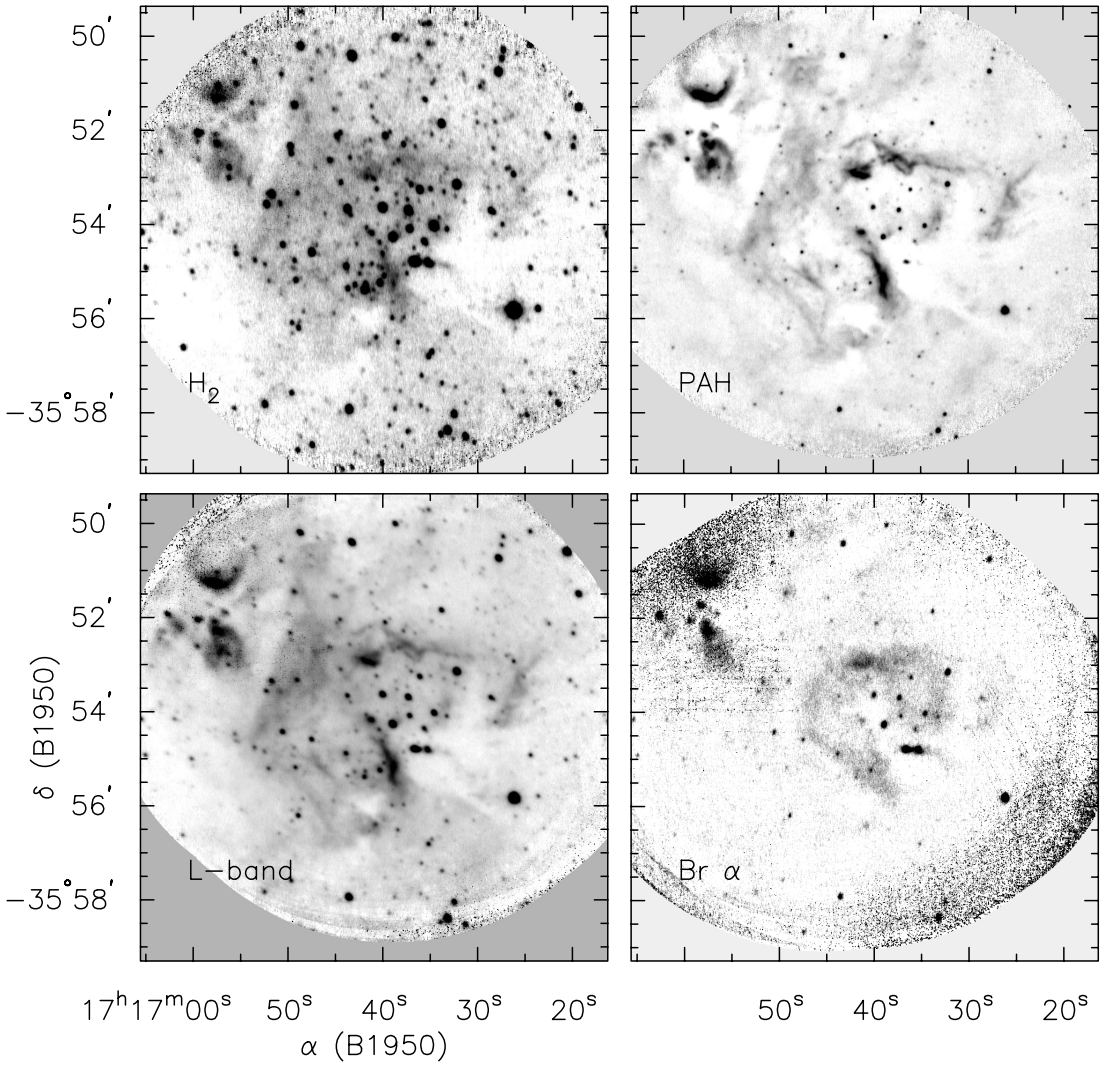

FIG. 5.—Images of the southwest quadrant of the molecular ridge, centered on NGC 6334 V. Clockwise, from top left: H_2 1–0 *Q*-branch 2.42 μm, PAH 3.3 μm, Brα 4.05 μm, and *L* band 3.5 μm.

on two near-IR sources, [SHM89] FIR-V 41 ($K = 8.5$, $17^h16^m39^s.0$, $-35°54'18''$: Straw, Hyland, & McGregor 1989; hereafter IRS 41) and 45 ($K = 12.6$, $17^h16^m38^s.9$, $-35°54'11''$: Straw et al. 1989; hereafter IRS 45) (see H_2 image in Fig. 5). The eastern side of this shell coincides with a region of optical H II nebulosity, but the remainder of the arc, including the brightest, northern section, does not have any corresponding optical nebulosity. The excitation of this shell has remained a puzzle since there is no OB star at its center; the sources IRS 41 and IRS 45 lack any radio counterparts and have been classified as B0 and B4, respectively (Straw et al. 1989). Jackson & Kraemer (1999) suggest that the various portions of the radio shell are physically distinct, with the northern and western sections associated with IRS 41 and the eastern section with two faint, unresolved radio sources, [RH96] NGC 6334 V R-E2 and R-E3 (at $17^h16^m36^s.6$, $-35°54'48''$ and $17^h16^m36^s.0$, $-35°54'50''$, respectively; hereafter R-E2 and R-E3; see L-band image in Fig. 5), which may be protostars.

The northern and western arcs show a classical PDR structure, with the 3.5 cm radio continuum (ionized gas) enveloped by an arc of [C II] 158 μm emission (neutral gas) and then by an arc of CO (2–1) emission (molecular gas), each arc separated by $\sim 20''$ (Jackson & Kraemer 1999). IRS 41 lies at the center of the arcs.

PAH and H_2 emissions also pervade this region, as seen in Figure 5. The emission regions are spatially coincident; however, their textures are quite different. The H_2 is diffuse and reasonably homogeneous through the emitting region. The PAHs, on the other hand, are filamentary, with bright ridges surrounded by more diffuse emission. Taking account of the different spatial resolution, both species are similar to the distribution of [C II] 158 μm emission (Jackson & Kraemer 1999). Thus, the H_2 and PAH emissions are most likely fluorescent in origin. Straw & Hyland (1989b) and Fischer et al. (1982) have previously reported H_2 emission from source V but claimed it was shocked. However, this interpretation arises from the low spatial resolution of their image, where a portion of the shell structure appears bipolar. It now appears more likely that the H_2 emission is fluorescent.

PAH emission arises from the very surface layer of PDRs (Allamandola, Tielens, & Barker 1989; Tielens et al. 1993), whereas H_2 emission extends to $A_v \sim 1$ from the surface. The intensity of H_2 emission is also dependent on the density of the gas. When the density is above critical ($\sim 10^5$ cm^{-3}), collisional de-excitation of fluorescently excited levels of hot molecular hydrogen leads to an excess in the $v = 1$ level and thus enhanced emission in $v = 1$ lines (Sternberg & Dalgarno 1989; Burton et al. 1990). Empirical evidence (e.g., Ryder et al. 1998; Allen et al. 1999) suggests that the brightest regions in fluorescently excited regions are also the densest regions and that their brightness is not simply the result of increased path lengths through the emitting gas along a sight line. Thus, for the H_2 emission to remain diffuse in source V, this suggests that the gas density is below critical ($\sim 10^5$ cm^{-3}) virtually everywhere. Based on ratios of CO (1–0), (2–1), and (3–2) lines, Kraemer & Jackson (1999) estimate the typical molecular cloud number density to be between 400 and 5000 cm^{-3}, well below the critical density. Only a limited region of gas seen in CS emission around the radio sources R-E2 and R-E3 is at substantially higher densities. The H_2 image morphology is thus consistent with this determination and, moreover, suggests there is little clumpy gas present outside the cores around the radio continuum sources.

A particularly bright filament of PAH emission $\sim 1'$ in extent (see PAH image in Fig. 5, centered at $17^h16^m39^s$, $-35°55'$) lies *within* the radio continuum shell (G351.20+0.70) and $\sim 30''$ east of the unresolved radio continuum sources R-E2 and R-E3. We suggest that this filament is not connected with the PDR associated with the eastern and northern arcs but instead is locally excited by R-E2 and/or R-E3. R-E2 is visible in the H_2, PAH, Brα, L-band, and M-band filters (see Fig. 5). It is also slightly extended east-west, which may be associated with the source R-E1. R-E3, $8''$ to its west, on the other hand, is visible in all these filters *except* the PAH filter. This indicates that the emission seen through the H_2 filter is continuum for R-E2 but is line emission for R-E3 (the bandpass of the PAH filter does not include the 3.1 μm ice-band feature). Source R-E3 thus appears to be a heavily embedded source with a compact H_2 (not H II!) region around it. Jackson & Kraemer (1999) have suggested that R-E2 and R-E3 may be protostars. This would imply that it is source R-E3 that is the protostar and that we are observing it at a very early stage of star formation, with either an outflow just forming or accretion shocks visible, producing shock-excited H_2 line emission.

4. CONCLUSIONS

We have conducted high spatial resolution imaging in the thermal infrared of H_2, PAH, and Brα lines and of L-band and M-band continua in the star formation complex NGC 6334, over a $30'$ field of view. These images have demonstrated the complex and diverse structures associated with gas in various stages of excitation in star-forming regions, including

1. shells of photodissociated gas, typically 1–1.5 pc across, outside bubbles of ionized gas which are 0.2–0.3 pc in size, surrounding the sites of massive star formation;
2. PAH emission associated with [C II] 158 μm line emission, rather than that of CO (2–1), demonstrating that the PAHs are excited in the warm photodissociation region rather than in the interior molecular cloud;
3. PAH emission that is spatially coincident with H_2 line emission, demonstrating that the bulk of the H_2 is fluorescent, rather than shocked; and
4. the morphology of the PAH emission that is filamentary in nature, as opposed to a more diffuse morphology for the H_2. This suggests the PAHs are emitting at the very edge of the PDRs, with the filaments indicating limb brightening on sight lines through edges of clouds, whereas the excited H_2 extends further into them. The fluorescently excited H_2 is generally at less than the critical density, $\sim 10^5$ cm^{-3}.

We have identified candidate massive protostars in NGC 6334 IV and V. In source V, the radio continuum source R-E3 appears to be a deeply embedded IR source, not visible at 2 μm, but with a compact H_2-emitting region around it (in addition to H II) and possibly the early signs of an outflow. The source R-E2 is also an embedded IR source with a compact H II region. In source IV, the mid-IR source KDJ-3 is an embedded IR source but has not yet reached the stage of producing an H II region and is not contributing to the excitation of the PDR emission. However, the source KDJ-2 is an IR source with a compact H II region

around it and is the likely source of excitation for the PDR emission. The diffuse arcs of PAH emission outside the radio and Brα shell of G351.20+0.70 in source V (as opposed to the bright arc near R-E2 and R-E3) are, on the other hand, likely excited by the source IRS 41.

These observations are the first images to be obtained of astronomical sources in the thermal infrared from Antarctica. They demonstrate the particular advantage that the Antarctic plateau provides for wide-field, high spatial resolution imaging at these wavelengths, as a result of the exceedingly dry and stable climatic conditions. These are the deepest images ever taken at these wavelengths with this spatial resolution, despite the modest size of the telescope. The results demonstrate that even a moderate size 2 m telescope will be able to take extraordinary deep images over wide fields of view from 2.4 to 5 μm. Such imaging will complement the narrow fields that the new generation of large ground-based telescopes and spacecraft will explore in depth, providing these facilities with a wealth of sources for further study.

This work is the result of the dedicated efforts of a great many people in JACARA and CARA. We especially wish to acknowledge the contributions of Mick Edgar and Andre Phillips in JACARA and Bill Ball in CARA. We thank David Malin for providing the color image of NGC 6334 shown in Figure 3. We are also grateful to the Australian Research Council and to the Australian Major National Research Facilities program for funding to support this program. We also thank the anonymous referee for helpful comments which added to the clarity of the paper.

JACARA is the Joint Australian Centre for Astrophysical Research in Antarctica, a cooperative venture between the University of New South Wales and Australian National University. CARA is the Center for Astrophysical Research in Antarctica, an NSF Science and Technology Center.

REFERENCES

Allamandola, L. J., Tielens, A. G. G. M., & Barker, J. R. 1989, ApJS, 71, 733
Allen, L. E., Burton, M. G., Ryder, S. D., Ashley, M. C. B., & Storey, J. W. V. 1999, MNRAS, 304, 98
Ashley, M. C. B., Burton, M. G., Storey, J. W. V., Bally, J., Briggs, J. W., Harper, D. A., & Lloyd, J. P. 1996, PASP, 108, 721
Burton, M. G., Hollenbach, D. J., & Tielens, A. G. G. M. 1990, ApJ, 365, 620
Chamberlain, M. A., Ashley, M. C. B., Burton, M. G., Phillips, A., Storey, J. W. V., & Harper, D. A. 2000, ApJ, 535, 501
Fischer, J., Joyce, R. R., Simon, M., & Simon, T. 1982, ApJ, 258, 165
Fowler, A. M., et al. 1998, Proc. SPIE, 3354, 1170
Gezari, D. Y. 1982, ApJ, 259, L29
Harvey, P. M., Hyland, A. R., & Straw, S. M. 1987, ApJ, 317, 173
Hereld, M., Rauscher, B. J., Harper, D. A., & Pernic, R. J. 1990, Proc. SPIE, 1235, 43
Jackson, J. M., & Kraemer, K. E. 1999, ApJ, 512, 260
Kraemer, K. E. 1998, Ph.D. thesis, Boston Univ.
Kraemer, K. E., Deutsch, L. K., Jackson, J. M., Hoffmann, W., Hora, J., Dayal, A., & Fazio, G. 1999, ApJ, 516, 817
Kraemer, K. E., & Jackson, J. M. 1999, ApJS, 124, 439
Kraemer, K. E., Jackson, J. M., Paglione, A. D. P., & Bolatto, A. D. 1997, ApJ, 478, 614
Loughran, L., McBreen, B., Fazio, G. G., Rengarajan, T. N., Maxson, C. W., Serio, S., Sciortino, S., & Ray, T. P. 1986, ApJ, 303, 629
Malin, D. F. 1993, A View of the Universe (New York: Cambridge Univ. Press), 91
McBreen, B., Fazio, G. G., Stier, M., & Wright, E. L. 1979, ApJ, 232, L183
Moran, J. M., Greene, B., Rodríguez, L. F., & Backer, D. C. 1990, ApJ, 348, 147
Nguyen, H. T., Rauscher, B. J., Harper, D. A., Loewenstein, R. F., Mrozek, F., Pernic, R. J., Severson, S. A., & Hereld, M. 1996, PASP, 108, 718
Phillips, A., Burton, M. G., Ashley, M. C. B., Storey, J. W. V., Lloyd, J. P., Harper, D. A., & Bally, J. 1999, ApJ, 527, 1009
Rodgers, A. W., Campbell, C. T., & Whiteoak, J. B. 1960, MNRAS, 121, 103
Rodríguez, L. F., Cantó, J., & Moran, J. M. 1982, ApJ, 255, 103
Ryder, S. D., Allen, L. E., Burton, M. G., Ashley, M. C. B., & Storey, J. W. V. 1998, MNRAS, 294, 338
Sternberg, A., & Dalgarno, A. 1989, ApJ, 338, 197
Straw, S. M., & Hyland, A. R. 1989a, ApJ, 340, 318
———. 1989b, ApJ, 342, 876
Straw, S. M., Hyland, A. R., & McGregor, P. J. 1989, ApJS, 69, 99
Stutzki, J., Stacey, G. J., Genzel, R., Harris, A. I., Jaffe, D. T., & Lugten, J. B. 1988, ApJ, 332, 379
Tielens, A. G. G. M., Meixner, M. M., van der Werf, P. P., Bregman, J., Tauber, J. A., Stutzki, J., & Rank, D. 1993, Science, 262, 86
Tielens, A. G. G. M., & Hollenbach, D. J. 1985, ApJ, 291, 722